Simultaneous Monitoring of Polymer and Particle Characteristics during Emulsion Polymerization

Alina M. Alb and Wayne F. Reed*

Physics Department, Tulane University, New Orleans, Louisiana 70115

Received December 13, 2007; Revised Manuscript Received January 17, 2008

ABSTRACT: Emulsion polymerization reactions constitute complex, nonequilibrium systems in which there is strong interaction between polymers, monomers, and the colloidal structures that mediate the reactions. A novel and general method was sought to monitor emulsion polymerization reactions. Instrumentation and methods were hence developed here to achieve, for the first time, simultaneous monitoring of the evolving characteristics of both the organosoluble components (monomer conversion, polymer molar mass, and reduced viscosity) and the colloidal components (particle size of monomer droplets and nucleated polymer particles). No empirical models were required for these determinations. This represents a new capability for the broadening ACOMP platform (automatic continuous online monitoring of polymerization reactions). The method was applied to free radical emulsion homopolymerization of methyl methacrylate and butyl acrylate over a wide monomer concentration range, with and without surfactant stabilization. A successful approach to soap-free emulsion polymerization (up to 15% solids) was developed and led to stable and uniform emulsions with no phase separation or coagulum buildup. Trends in the polymer characteristics were cross-correlated with evolving colloid particle distributions, and the model of mass transfer from large monomer droplets (microns) to much smaller, nucleated particles which are the loci of polymerization (ca. 100 nm) was confirmed. This was seen in the disappearance of the large monomer droplets and appearance of polymer particles during monomer conversion. Results were cross-checked with offline multi-detector size exclusion chromatography, dynamic light scattering, and cryogenic transmission electron microscopy. This new ACOMP approach should be widely applicable to monitoring many types of emulsion polymerization reactions.

Introduction

Emulsion polymerization was developed for producing polymers with unique properties and because of environmental considerations. Since properties such as copolymer composition, molecular weight distribution, branching, particle morphology, and size distribution depend on the evolution of the complex and delicate balance between the emulsion components, it is critical to understand how these variables affect the emulsion end products in order to develop accurate predictive models and/or reaction control schemes.

Although the reaction medium in emulsion polymerization remains at low viscosity, factors such as instability of the lattices and other nonequilibrium phenomena, complexity of the materials produced, and multifaceted properties requiring multiple characterization approaches make the task quite challenging.

Characterization of organosoluble component characteristics and colloidal size distributions have typically been carried out using different sampling procedures and disparate instrumentation, often in different laboratories. This piecewise and tedious approach makes it difficult to assess and quantitatively evaluate the characteristics and interrelationships of these complex, nonequilibrium colloidal/polymer systems.

Existing online methods depend on the accuracy of the calibration and on the many parameters involved in the models used. Another frequently reported issue is the quality of the emulsions, which are often inhomogeneous and unstable and lead to coagulum buildup on the reactor components and on the sensors used to monitor changes in the reaction medium.

Automatic continuous online monitoring of polymerization reactions (ACOMP) was introduced in 1998 as a comprehensive and versatile platform for monitoring monomer and comonomer conversion, and polymer molecular mass and intrinsic viscosity during the reaction, to understand the kinetics and reaction mechanisms and, potentially, to control reactions to optimize synthesis. Initially used to monitor and study homogeneous phase systems,[1−4] the technique was adapted recently to the monitoring of inverse emulsion polymerization.[5]

A new advance with regard to the instrumentation and methods available for online monitoring of heterogeneous polymerization reactions is presented here in which the two different aspects of the emulsion polymerization reaction are monitored: (1) Monitoring the organosoluble components, including polymer and monomer characteristics, is achieved by diluting the reactor content continuously and automatically throughout the reaction with an organic solvent miscible with water (tetrahydrofuran, THF) to create a homogeneous, dilute solution. From this, polymer weight-average molar mass, M_w, and intrinsic viscosity, $[\eta]_w$, are obtained as well as monomer conversion. In the case of copolymers, average composition drift and distribution will be measurable (future work). (2) Monitoring the colloidal components, such as the emulsions and nucleated polymer particles, is achieved by diluting the emulsion with H_2O throughout the reaction and measuring with suitable particle sizing detectors.

Thus, this approach offers a unified means of monitoring colloid/polymer characteristics and gives information about both the polymer and particle evolution, allowing one to make correlations between key features of the two aspects of the emulsion polymerization process. Online monitoring of both particle and polymer characteristics should allow for studies of reaction kinetics, predictive and active reaction control, and also the ability to observe deviations and unexpected phenomena.

Emulsion Polymerization Background

Often, the results of emulsion polymerizations can be rationalized according to more than one theory. Hence, advances in monitoring emulsion polymerization reactions will furnish more accurate and integrated information, allowing thorough evaluation of different models.

* To whom correspondence should be addressed.

10.1021/ma7027825 CCC: $40.75
Published on Web 02/21/2008

According to classical emulsion polymerization theory, the three intervals describing the process are (1) formation or "nucleation" of the particles in which polymerization chiefly occurs, (2) particle growth due to the polymerization reaction, which leads to an increase in particle surface area, and (3) monomer transport from large monomer droplets to the nucleated polymer particles, where they are converted, causing the monomer droplets to shrink and disappear as the monomer is converted to polymer.

Several mechanisms were formulated to explain nucleation. The primary particle formation takes place by entry of a free radical into a micelle[6,7] (micellar nucleation) or by homogeneous nucleation[7,8] of the oligomeric free radicals in the aqueous phase. If an appropriate cosurfactant is used, smaller and more stable monomer droplets become the primary locus of particle nucleation[9] (miniemulsion systems). Once the primary particles are formed, they grow as the monomer within gets converted to polymer or by particle coagulation.[10]

On the basis of Harkins' theory, the small amount of monomer solubilized in micelles represents the principal locus for the nucleation and leads to polymer growth by capturing monomer transported through the aqueous phase. Hence, the monomer droplets act merely as reservoirs, from which monomer diffuses into the aqueous phase. The micellar nucleation theory does not apply to all emulsion systems, those involving more hydrophilic monomers being an example. Determination of the particle size distribution may help to discern different mechanisms.

Miniemulsion polymerization allows high molecular weight and polymerization rates to be achieved, with the possibility of using water-insoluble reactants, minimizing mass transfer through the aqueous phase. Despite several studies on the kinetics of the miniemulsion polymerization,[11,12] the mechanism of the reaction in terms of droplet nucleation, effect of the homogenizer, and surfactant−cosurfactant combination on the droplet size distribution is not well understood, and conflicting results have been reported.

Composition control can be obtained by open- or closed-loop approaches. The first is operated with a predefined monomer addition profile under starved conditions,[13] by model prediction[14] or iterative approaches.[15] The more reliable sensors used make the close-loop control systems a more robust way to control the polymerization rate. Densimetry,[16] ultrasound velocity,[17] and calorimetry[18,19] are among the most commonly used indirect sensors, which relate a certain parameter in the reactor to concentration, whereas gas chromatography,[20] UV spectroscopy,[21] near-IR,[22–24] mid-IR spectroscopy,[25,26] ATR-Fourier transform IR spectroscopy,[27] and Raman spectroscopy[28,29] are direct sensors which monitor the reaction features.

There are several reviews about online monitoring methods for emulsion polymerization.[20,30–32] Among the noninvasive techniques, calorimetry[33,34] is used for monitoring the polymerization rate by estimating the heat of polymerization and the overall heat-transfer coefficients. Spectroscopic techniques are widely used in monitoring monomer/polymer properties.[35] Raman spectroscopy is an attractive route,[36–38] but no direct relationship between the absolute intensity and monomer concentration can be made and calibration models are required.[39] Multivariate calibration techniques have been developed to relate the spectra with the concentration of each monomer.[40] Near-IR spectroscopy has also been used to estimate monomer and polymer content and polymer particle size.[41,42]

A large drawback of the in-situ methods is that they work in concentrated reaction environments, and hence the signals obtained usually must be interpreted using chemometric or other empirical calibration schemes. Because emulsions also scatter electromagnetic radiation, these effects can interfere with, and often even overwhelm, the portion of the signal due to monomeric absorption. A further possible problem with the in-situ approach is that such probes can be fouled or damaged by the reaction environment, causing large shifts, or complete breakdown, of the empirical calibration schemes.

A significant advantage of the online method presented here vis-à-vis the in-situ methods is that the ACOMP "front end", comprising an ensemble of pumps, dilution, and conditioning stages, provides a continuous, dilute, and well-conditioned sample stream to the sensitive detector train. This allows for absolute, model-independent determination of quantities such as conversion, composition, and molar mass distribution and does not subject the detectors to potentially damaging environments.

Particle size and particle size distribution (PSD) strongly affect end-product properties and applications. There are, however, still issues regarding accurate offline PSD determination of the latex particles,[43] but recent advances have been made.[44,45]

Experimental Section

A crucial step in preparing monomer emulsion and keeping it stable is the mixing. The authors are not aware of online monitoring techniques based on continuous withdrawal of the emulsion from reactor with continuous dilution and conditioning. This is a very challenging approach and involves overcoming several technical difficulties. To start, it requires a uniform distribution of the emulsion components for a relatively long time (30–40 min) before the reaction starts. During this time, phase separation must be avoided, so that a constant, stable, and reproducible (emulsified) monomer baseline is acquired.

After many approaches and trials, a Ross homogenizer was used at 1800 rpm to achieve good mixing before and throughout the reaction. The high stirring rate is required especially in the case of the soap-free emulsion experiments reported here. For the emulsions in which surfactant is present, a lower stirring could be used. However, the monomer emulsion has to be homogenized at high rpm prior to being added into the reactor; otherwise, phase separation occurs and/or polymerization proceeds with different rates.

The polymerization reactions were performed in a 500 mL reactor purged continuously with N_2. The initiator, potassium persulfate ($K_2S_2O_8$), and the monomers, methyl methacrylate (MMA) and butyl acrylate (BA), were used as received from Aldrich.

The differential refractive index increment dn/dc values of the homopolymers used in M_w computations were 0.084 for pBA and 0.100 for PMMA in tetrahydrofuran (THF), based on results from previous work.[3,4]

The ACOMP "Front End" for Extraction, Dilution, and Conditioning. Considerable trials and failures were made, using several types of pumps and mixing chambers, before arriving at an operable extraction and dilution scheme. Two streams were extracted continuously and simultaneously from the reactor, each via a Fluid Metering Q pump. The first stream reached a low-pressure mixing chamber (LPMC, ∼5 mL) where it was diluted with THF, continuously supplied in the LPMC with a HPLC pump. THF was chosen as dilution solvent since it is miscible with all the emulsion components (water, monomer, and polymer), and no precipitation occurs at any point in the tubing or LPMC/detectors. Another HPLC pump was used to withdraw the diluted emulsion and continuously pump it into a second LPMC, where it was diluted again with THF to produce a dilute solution of polymer and monomer for characterization, in a range of 0.5–1 g/mL total concentration of polymer plus monomer, depending on the particular experiment. The second stream, continuously withdrawn from the reactor, was diluted with H_2O, depending on the experiment, from 100 to 500 times in two dilution stages in a similar manner to

conserve the colloidal morphology of the emulsions in order to monitor particle number and size distribution.

The delay time between sample extraction and measurement by the detector train depends on the conditions used and typically runs from 3 to 5 min. The response time is typically in this same range and is defined as the half-time for the detectors to equilibrate to a sudden step function change in the reactor (e.g., addition of a detectable reagent, such as an initiator).

Different detectors were used, depending on the polymer/particle features monitored.

Polymer/Monomer Side. A 2 μm inline frit was included between the final pump and the detector train, consisting of a custom-built single capillary viscometer, a Waters 410 refractive index detector (RI), a Brookhaven Instruments Corp. BI-MwA multiangle light scattering (MALS) detector, and a Shimadzu Corp. SPD-10AVvp ultraviolet/visible spectrophotometer (UV) detector. There was no coagulum buildup at any time on the reactor walls or in the tubing or inline filters, which reflects on the quality of both the emulsion and the procedure used in the dilution/conditioning process. The reactor emulsion diluted with THF was passed through detectors at 1 mL/min during the reaction. Detectors sampled the diluted, flowing stream every 2 s.

The well-known Zimm approximation,[46] to second order in polymer concentration c (g/cm^3), shows the quantity $Kc/I(q,c)$, where $I(q,c)$ is the excess Rayleigh scattering ratio, can be approximated by

$$\frac{Kc}{I(q,c)} = \frac{1}{MP(q)} + 2A_2c + [3A_3Q(q) - 4A_2MP(q)(1 - P(q))]c^2 \quad (1)$$

where M is polymer molar mass, A_2 and A_3 are second and third virial coefficients, respectively, and $P(q)$ is the particle form factor. $Q(q)$ involves a sum of Fourier transforms of the segment interactions that define A_2 and A_3. This equation forms the basis of the Zimm plot, which, at low concentrations and for $q^2\langle S^2\rangle_z \ll 1$ can be written, for a polydisperse polymer population, as

$$\frac{Kc}{I(q,c)} = \frac{1}{M_w}\left(1 + \frac{q^2\langle S^2\rangle_z}{3}\right) + 2A_2c \quad (2)$$

which directly permits determination of M_w, A_2, and the z-averaged mean square radius of gyration $\langle S^2\rangle_z$. K is an optical constant, given for vertically polarized incident light by

$$K = \frac{4\pi^2 n^2 (\mathrm{d}n/\mathrm{d}c)^2}{N_A\lambda^4} \quad (3)$$

where n is the solvent index of refraction, λ is the vacuum wavelength of the incident light, dn/dc is the differential refractive index for the polymer in the chosen solvent, and q is the usual scattering wave vector $q = (4\pi n/\lambda)\sin(\theta/2)$, where θ is the scattering angle.

It is important to note that within the limit of approximation of eq 2 ($q^2\langle S^2\rangle_z \ll 1$), there are no assumptions about particle shape or morphology, and it hence can be used to determine M_w, A_2, and $\langle S^2\rangle_z$ for random coils, cross-linked, branched, rodlike polymers, etc., in model-independent fashion.

Particle Side. The emulsion, twice diluted with H_2O, was passed at 2 mL/min through a particle size detector (Mastersizer 2000, Malvern Instruments), without filtration. Again, the cleanliness and stability of the emulsion allowed this approach. It is further important to point out that where scattering measurements on massive scatterers are made (e.g., polymer latex particles), one does not encounter the type of distortions in data due to low levels of "dust" and other contaminants that are crucial when measuring weakly scattering particles (e.g., dilute solutions of low to medium mass polymers). Measurements were made every 35 s, and analyzed with the Malvern particle size analysis software, based on Mie scattering theory.[47] Mie theory gives exact results for the angular distribution of scattered light. When the scatterers are uniform spheres, these distributions depend only on the indices of refraction of the solvent and sphere, the wavelength of the incident light, and the sphere diameter. The Mastersizer 2000 performs the inverse scattering problem by taking the measured angular distribution of light using red and blue laser sources and the indices of refraction to compute the approximate size distributions that yield the measured angular scattering distributions. The values of n_p for pBA and pMMA particles were taken as 1.464 and 1.489, respectively, and 1.333 for water. Different means and moments of the particle size distribution are calculated using the definitions and terminology of the British publication BS2955:1993. Thus, D(v,0.5), D(v,0.1), and D(v,0.9) are the sizes (in μm) below which 50% (mass median diameter), 10%, and 90% respectively, of the sample lies. D[4,3] is the volume mean diameter, and D[3,2] is the surface area mean diameter. In the case of the emulsions and polymer latex particles the spherical approximation is quite appropriate, since no shape asymmetry is expected. Cryogenic TEM results (below) also show that the latex particles are spherical to a high level of approximation.

Scheme 1. Schematic of the "Front-End" Instrumentation Used for Simultaneous Monitoring of Colloid and Organosoluble Component Characteristics during Emulsion Polymerization Reactions

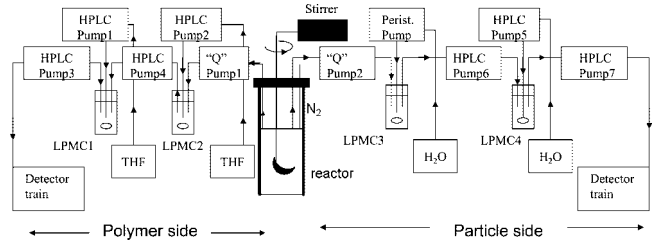

Because dilution of the surfactant containing emulsions might be sensitive to whether or not there is SDS in the dilution solvent, it was verified that diluting the polymer particle end product with or without SDS in the water does not affect the size measurements. There can be an effect on the monomer droplets, but these are very broad and ill-defined distributions anyway and they are not to be taken literally. The important point is that the polymer particles in this work are not sensitive to the type of dilution.

Scheme 1 shows a simplified schematic of a typical setup for the extraction/dilution of the reactor content before reaching the detector train. The tubing used in all parts of the system had an internal diameter of 0.02 in.

Conventional cross-checks on ACOMP results for molar mass and monomer conversion were provided by multidetector size exclusion chromatography (SEC) measurements made on aliquots withdrawn manually from the reactor during the polymerization reaction. The SEC system used a Shimadzu HPLC pump, two PLgel 10μ MIXED-B columns in series, and similar RI, MALS, UV, and viscometer detectors as in the ACOMP system. There was a 0.45 μm inline frit filter before the SEC column. Similarly, dynamic light scattering (DLS) was used to cross-check the ACOMP particle sizing results provided by the Mastersizer. DLS measurements were made on a Brookhaven Instruments Corp. 90Plus particle sizer and analyses made on the basis of the Stokes–Einstein relation for hydrodynamic radius derived from the intensity autocorrelation function,[48] expanded in terms of cumulants.[49] Additionally, cryogenic transmission electron microscopy (Cryo-TEM) was used to visualize the nucleated polymer particles.

Results

Verification of Rapid Particle Dissolution in THF. The fact that the emulsion and polymer latex particles actually dissolved within the time required for dilution by the ACOMP front end was verified by using the recirculation technique originally employed for measuring the time for dissolution of inverse emulsions.[5] In this method THF is continuously recirculated from a solvent reservoir through the detector train with a peristaltic pump. A few drops of emulsion are added to the

Table 1. List of Parameters for Emulsion Polymerization Reactions of BA and MMA[b]

no.	% mass[a]	C_M (M)	$C_M/C_{initiator}$(M/M)	C_{SDS} (M)	$M_{w@f=1}$ (g/mol)	$\eta_{r,w}$ (cm^3/g)	T (°C)
1 MMA	4.7	0.458	290	0	1.80×10^5	150	70
2 BA	3.5	0.270	140	2.244×10^{-3}	1.65×10^7	680	55
3 MMA	4.7	0.458	299	8.075×10^{-3}	2.50×10^6	400	70
4 BA	14.0	1.110	199	0	5.00×10^6 [c]	760	70
5 BA	35.0	2.529	304	6.549×10^{-3}	1.45×10^7	1250	70

[a] (g of monomer) × 100/(g of reactor solution). [b] $K_2S_2O_8$ was used as initiator, except for experiment 2, where *tert*-butyl hydroperoxide and sodium formaldehyde sulfoxylate were used. [c] Lower bound on M_w from $I(\theta = 35°)/Kc$.

reservoir to make the combined concentration of monomer and polymer similar to that used in the ACOMP dilution stage. The response of the UV, RI, and MALS detectors then monitor the dissolution of the particles into homogeneous solution. In this work it was found that the monomers were homogenized in less than 20 s. The polymers were solubilized also in less than 20 s, but it could take up to a few hundred seconds for the MALS signal to reach a stable plateau, possibly indicating a period for the chains to disentangle from each other after the polymer particles are dissolved. The delay time between extraction from the reactor and reaching the detector train was between 2 and 6 min, depending on the details of the dilution stages and flow rates. Likewise, the system response time due to the dual mixing stages was between 2 and 4 min, again depending on mixing details. The response time is defined as the reciprocal of the exponential rate at which a step function applied to the system reaches steady state (e.g., a rapid injection of initiator or other detectable molecule into the reactor can be used to measure this).

Results from several emulsion polymerization reactions of methyl methacrylate (MMA) and butyl acrylate (BA) are reported next. Since the goal of this work is to establish novel online instrumentation and methods in the case of emulsion polymerization, a wide range of reaction conditions were covered. The reactions conditions are shown in Table 1. Each experiment constitutes a general example in the category reported and could lead to a more detailed study in terms of kinetics and reaction stages. The point was to demonstrate the efficiency and versatility of the online method as a powerful tool for studying polymerization kinetics in heterogeneous phase polymerization reactions. It is beyond the scope of this work to delve into detailed kinetics, interpretations, and models of the data for any of the experiments.

In the following, stable and coagulum-free emulsions were produced for reactions with and without surfactant (SDS) added, from the dilute regime (4% monomer by mass) to high yield reactions (35% monomer by mass).

Low Concentration Regime: MMA Reaction with SDS. Figure 1 shows raw data from the "polymer side" (Scheme 1) for a typical reaction, no. 3 in Table 1. A continuous, dilute, homogeneous stream from the emulsion liquid in the reactor was created, as described in the Experimental Section. First, the solvent baseline (SDS solution diluted with THF) ran from 0 to 1000 s, at which point the MMA was added in the reactor, homogenized with the Ross homogenizer, and the MMA emulsion baseline started; the RI and UV (225 nm) responded to the dn/dc of MMA in THF and the double bond absorbance, respectively. The viscosity and LS were unaffected by the dilute flow of monomer. The reaction was initiated around 2500 s and proceeded to completion by 4000 s. During this time a small stream of the reactor content was withdrawn and diluted continuously before reaching the detector train. A small increase was observed in the UV signal when initiator was added, whereas the other detectors were insensitive to its presence. The strong increases in LS and viscosity during conversion monitored the increasing polymer concentration, whereas the decrease in UV monitored the loss of double bonds and hence conversion.

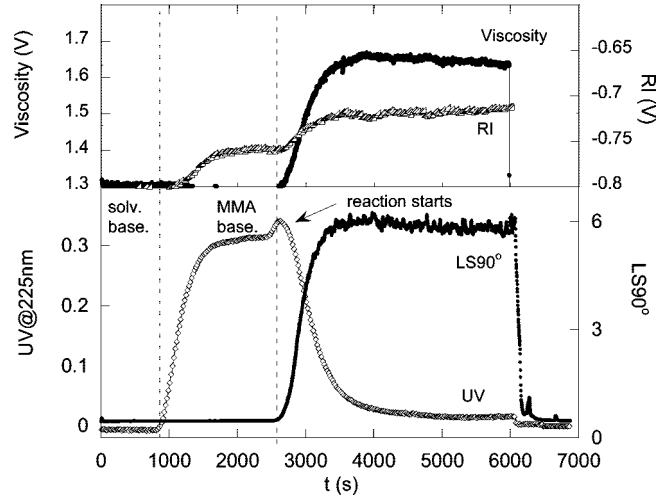

Figure 1. Raw ACOMP signals (arbitrary units) for LS90°, viscosity, RI, and UV at 225 nm during experiment 3 in Table 1 (MMA polymerization).

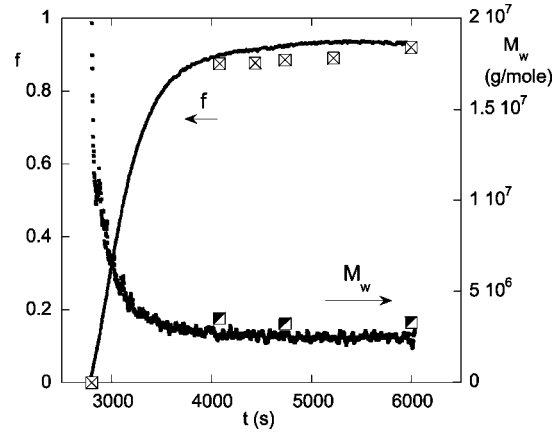

Figure 2. Evolution of the fractional monomer conversion, f, and the polymer mass, M_w, during the polymerization reaction (experiment 3). Discrete points are SEC results from manually withdrawn reaction aliquots.

The RI increased since dn/dc of pMMA is higher than that of MMA. After 6000 s solvent was run through the detectors, and the initial baselines were recovered.

The evolution of the monomer conversion, f, and the polymer weight average mass, M_w, during the polymerization reaction 3 are shown in Figure 2 vs time, computed from raw data above according to established ACOMP procedures.[1,2] The large squares are SEC results from discrete measurements on samples manually withdrawn from the reactor during the reaction, in agreement with ACOMP values, although the reactor was not manually sampled quickly enough to capture the early phases of conversion and M_w.

Weight-average reduced viscosity, $\eta_{r,w}$, and M_w are shown vs monomer conversion in Figure 3. Both quantities display the characteristic decrease vs conversion that is typical of free

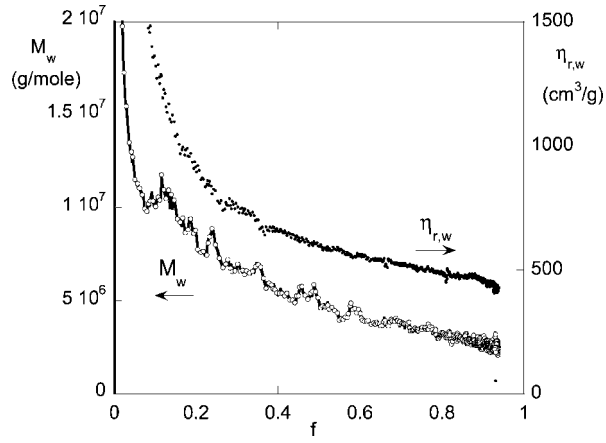

Figure 3. Weight-average reduced viscosity, $\eta_{r,w}$, and M_w vs monomer conversion for experiment 3.

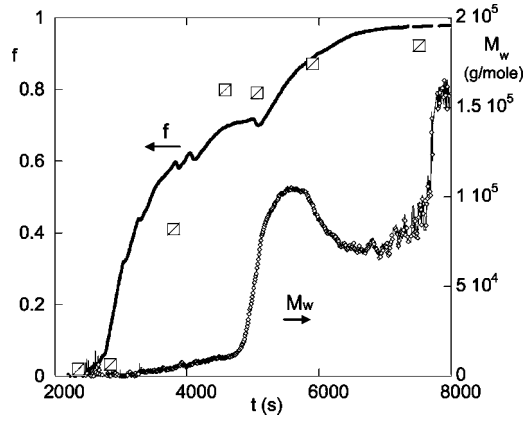

Figure 4. Evolution M_w and fractional monomer conversion, f, in a surfactant-free emulsion polymerization of MMA (no. 1, Table 1). SEC conversion data are shown from aliquots withdrawn from reactor during the polymerization.

radical homopolymerization when the initiator decomposes slowly compared to the total time of conversion, and there are no significant chain transfer processes.[2] In this case, the persulfate half-life at this temperature (70 °C) is 20.9 h. Higher M_w and $\eta_{r,w}$ were found in the case of the emulsion reactions performed with added surfactant under otherwise similar conditions.

ACM ramps on end products (not shown) displayed very little dependence of $\eta_{r,w}$ on polymer concentration c_p. Thus, the values of $\eta_{r,w}$ shown in Figure 3 and in the tables are very close to the weight-average intrinsic viscosity, $[\eta]_w$.

Low Concentration Regime: MMA Polymerization without Surfactant. This type of reaction posed many technical challenges, and there are few successful studies reported in the sparse soap-free emulsion polymerization literature. As mentioned above, high stirring with the homogenizer was required in order to maintain a stable emulsion, to prevent phase separation and subsequent coagulum buildup.

Data from a surfactant-free emulsion polymerization of MMA (reaction 1 in Table 1) are shown in Figure 4. The reaction appears to have two separate conversion phases, each with approximately the same rate. This ACOMP conversion result was very roughly confirmed by independent SEC measurements, shown as discrete points in Figure 4. The deviations of the SEC resulting from ACOMP are due to noise and baseline issues in the SEC data themselves. At any rate, the biphasic conversion is not clearly seen with just the SEC data. In the first conversion phase M_w is very small, $<10^4$ g/mol, but rapidly jumps to over

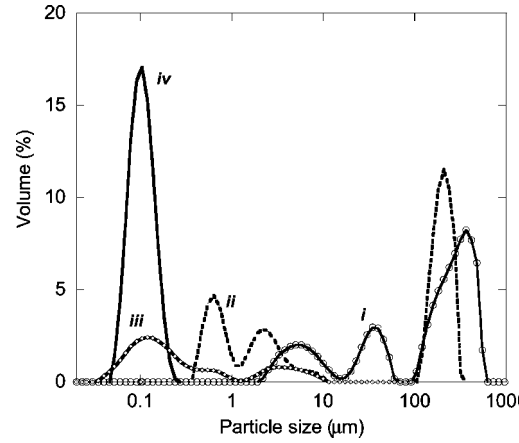

Figure 5. Four selected particle size distributions taken from the distributions measured every 35 s during reaction 2 (Table 1).

10^5 g/mol in the second conversion phase, after which there is some decrease, followed by a further increase. SEC molecular weight distributions (discussed below) showed two populations, each around the value of the corresponding ACOMP phase of conversion. A possible explanation for the two-phase conversion behavior could reside in the relatively high solubility of MMA in H_2O, which leads to a significant amount of polymerization during the first phase in the homogeneous aqueous solution at low monomer concentration and relatively high initiator concentration, leading to small (and/or aqueous insoluble) chains The second phase might occur after nucleation of particles in which heterogeneous phase polymerization occurs, which generally produces larger polymers than corresponding homogeneous phase reactions. More thorough investigations, beyond the scope of the current work, would have to be done to elucidate the origin of the bimodality and peculiar features monitored.

Such two-phase behavior was not observed for low concentration BA reactions without surfactant, probably because of the much lower aqueous solubility of BA compared to that of MMA.

Particle Size Distribution—Examples; Low Concentration BA with SDS. Figure 5 shows selected particle size distributions (from those taken continuously every 35 s) from the "particle side" (Scheme 1) for four different times during reaction 2. Initially (distribution i), there are only monomer droplets, with three modes, all above 1 μm. These droplets themselves are unstable in time and will eventually phase separate if the reaction is not initiated. Before the reaction, as seen in distribution i, there are no submicron particles. Very shortly after the reaction begins (distribution ii), the two smaller distributions from distribution i shift to lower values. Further, in the conversion (distribution iii) there is now a mode near 100 nm, which corresponds to the polymer latex particles, the largest mode at 200 μm has disappeared completely, and there are only remnants of the other two larger modes. Finally (distribution iv), only the mode at 100 nm, corresponding to the polymer latex, remains. The progression of these distributions hence corresponds at least qualitatively to the classical model of emulsion polymerization in which the large monomer droplets are consumed and much smaller, stable polymer latex particles grow at their expense.

High Concentration Regime: BA Reactions without and with SDS. The ACOMP monitoring approach yielded good data for the industrial-level high solids reactions with and without surfactant stabilization. The polymers produced, however, were more massive than in the low concentration reactions. Figure 6 shows the evolution of the lower bound on the polymer mass, $M_{w,35}$, with conversion during a surfactant-free polymerization

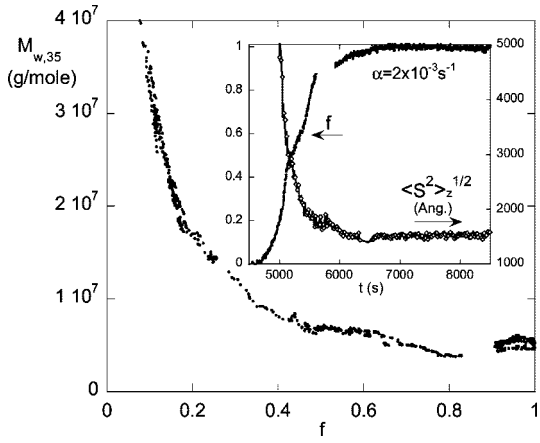

Figure 6. Evolution of the minimum lower bound on polymer mass, $M_{w,35}$ (see text for explanation), vs f during the polymerization reaction 4. $\langle S^2\rangle_z^{1/2}$ and f vs time are shown in the inset.

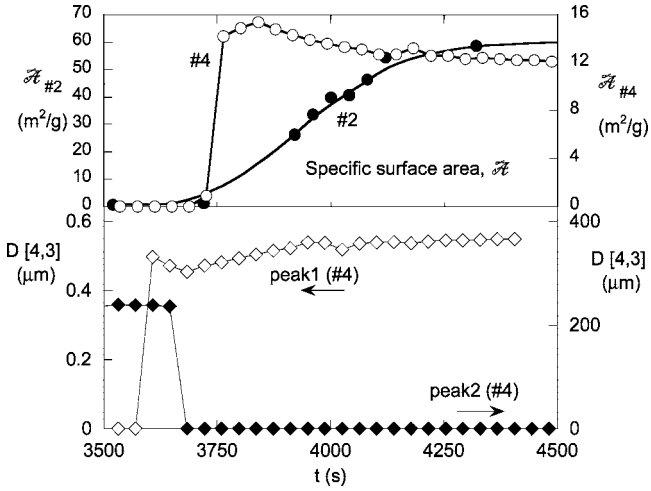

Figure 7. Evolution of the specific surface area (upper) for reactions 2 and 4. The volume-weighted mean diameter, $D[4,3]$, for two modes in the particle size distribution (lower) for reaction 4 (Table 1).

reaction (reaction 4, Table 1). Similar to the low concentration reactions, typical free radical homopolymerization behavior for M_w is observed. $M_{w,35}$ represents the value of $I(\theta)/Kc$ from eq 1 at a scattering angle of 35°. The polymers in the early phase of the reaction are so large that it is impossible to extrapolate the data to 0° with any accuracy. Hence, the true M_w will be higher than the values shown in Figure 6, and $M_{w,35}$ is a lower, measurable bound on this mass. The M_w values in Table 1 are the values from extrapolation to $\theta = 0°$, except for reaction 4, for which the lower bound from $\theta = 35°$ is given.

In the inset to Figure 6, $\langle S^2\rangle_z^{1/2}$ (in angstroms) and f are shown vs time. The conversion shows approximate first-order kinetics with a rate of 0.0020 s^{-1}. The values of $\langle S^2\rangle_z^{1/2}$ for the lower bound M_w values in Figure 6 are in reasonable agreement with the relationship between $\langle S^2\rangle^{1/2}$ and M from SEC, discussed below.

Figure 7 displays results from the particle sizing. In reaction 4 there were two main size modes, one below 1 μm and the other at several hundred microns. The volume-weighted mean diameter, $D[4,3]$, for each of the two modes in the particle size distribution for reaction 4 is shown in Figure 7 (lower portion). Peak 1 is for the small population of growing, nucleated polymer latex particles, and peak 2 is for the large mode. The larger particles are monomer droplets. A short time for particle growth (all data integrated by volume) is suggested by the rapid

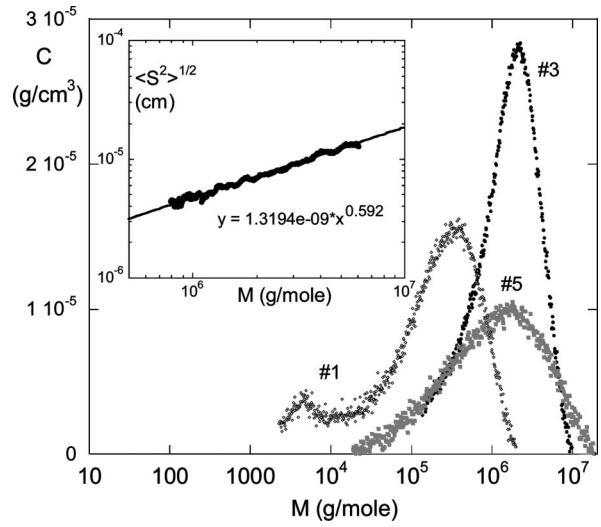

Figure 8. SEC molecular weight distributions for reactions 1, 3, and 5 (Table 1). The inset shows the scaling law between $\langle S^2\rangle^{1/2}$ vs M (from experiment 3).

appearance of the mode corresponding to the nucleated polymer particles and the decrease in all the other size averages.

The evolution of the specific surface area is shown for experiments 2 and 4 in the upper part of Figure 7 and is taken over all the modes in the distribution.

The reactions conditions were chosen to highlight polymerization kinetics and did not focus on the nucleation stage, which occurred very quickly. Nonetheless, the increase in specific surface area observed at the outset of nucleation indicates formation of small polymer particles at the expense of the low surface/volume large particles and furnishes a trend in particle size evolution. Additionally, in the case where high monomer concentration is used, a subsequent small decrease in specific surface area was observed in Figure 7, indicating the tendency of the particles either to aggregate or to individually swell. This effect was not seen in the low concentration reactions. As an example, the evolution of specific surface area for experiment 3 shows it gradually increasing and reaching a maximum.

The path opened by the online approach presented here will allow one to measure kinetics and to gather more information about the nucleation stage to be characterized in appropriate conditions, especially at lower monomer concentration.

Relationship of SEC Results to ACOMP. Figure 8 shows molecular weight distributions for reactions 1, 3, and 5. The bimodality in no. 1, a surfactant-free reaction, corresponds to the values of M_w found in the biphasic conversion from ACOMP, shown in Figure 4. The other distributions are monomodal, in agreement with the ACOMP monitoring.

The inset to Figure 8 shows the SEC result for $\langle S^2\rangle^{1/2}$ vs M (experiment 3), yielding the power law

$$\langle S^2\rangle^{1/2}\,(\mathrm{cm}) = 1.32\times10^{-9}\,\mathrm{M}^{0.592} \qquad (4)$$

The exponent of 0.592 is typical of a random coil in a good solvent, i.e., with considerable positive excluded volume.

It was shown by several groups that branching occurs in emulsion polymerization of alkyl acrylate due to the intra- and intermolecular chain transfer to polymer.[50,51] Polymer networks can be formed especially if monomers with two or more double bonds are polymerized.

There is evidence of branching in the case of the BA polymerization reactions, at low and high concentration. As an example, shown in Figure 9 are $\langle S^2\rangle^{1/2}$ vs M (above) and $[\eta]$ vs M (below) for the end product of reaction 5 and a polystyrene standard ($M_p = 1 \times 10^6$ g/mol). The low values of the exponent

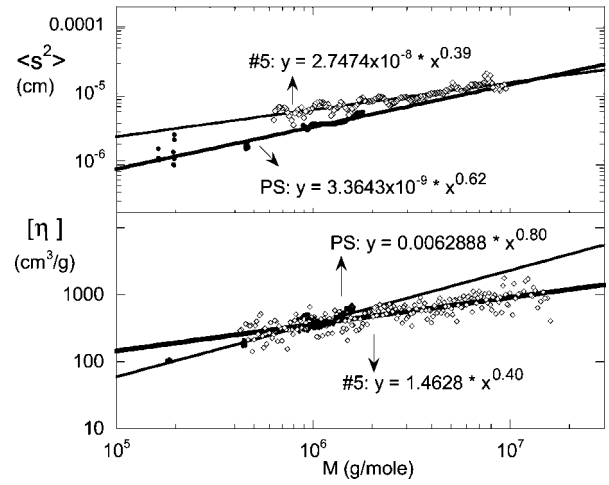

Figure 9. SEC power laws of $\langle S^2\rangle^{1/2}$ and $[\eta]$ with M in the case of the pBA end product of reaction 5 compared to the same parameters for a polystyrene standard ($M_p = 1 \times 10^6$ g/mol).

for $\langle S^2\rangle^{1/2}$ vs M and Mark–Houwink exponents for pBA case indicate branching.

For the low concentration reactions (nos. 1−3 in Table 1), there was excellent agreement between M_w, $[\eta]_w$, and $\langle S^2\rangle_z$ as determined by both ACOMP and SEC. For the high concentration cases (nos. 4 and 5), however, there were considerable differences between the results. Namely, M_w and $[\eta]_w$ from ACOMP are significantly higher than the SEC values. Nonetheless, there is good agreement between the $\langle S^2\rangle_z^{1/2}$ vs M_w by ACOMP and eq 4 from SEC for these cases. That is, when the M_w values from nos. 4 and 5 are used in eq 4, they yield values of $\langle S^2\rangle$ in good agreement with the $\langle S^2\rangle_z$ measured by ACOMP for those large masses. This strongly suggests that ACOMP is monitoring large, well-dispersed polymers from the reactor but that SEC does not detect these.

One of the leading possibilities for the discrepancies between ACOMP and SEC is that high shear in the SEC system leads to degradation of the very large chains, thus leading to artificially smaller masses. The ACOMP system has a 2 μm frit in line and relatively low shear rates through most of the tubing. In SEC, in contrast, the polymers are forced through columns with a wide range of internal pore sizes where the polymers are subject to high shear. Additionally, there was a 0.45 μm inline frit before the columns. In fact, in the first ACOMP work with inverse emulsions it was found that the very high mass polyacrylamide was very sensitive to shear rate effects in both SEC and ACOMP, and the ACOMP was subsequently and specifically adapted to low shear conditions.[5] Another possibility is that the very high mass polymers get trapped in the columns. There was no increase in SEC pump pressure, however, so that if there were polymers trapped, the amount would have been small.

Yet another possibility is that as the latex particles swell and/or coalesce in the high concentration reactions the ACOMP dilution process does not fully break down the particles, resulting in some residual high mass polymer aggregates or entanglements. One argument against this is that in all cases M_w by ACOMP *decreases* with conversion, so that it is not likely that such a decrease corresponds to aggregates from increasingly entangled polymers. Also, entanglements of polymers would be expected to yield lower $\langle S^2\rangle$ for a given mass, yet the ACOMP relationship between $\langle S^2\rangle_z$ and M_w follows the eq 4 relation between $\langle S^2\rangle$ and M fairly well. Finally, the direct emulsion dissolution experiments described above indicated polymer disentanglement within the time frame of the ACOMP dilution process.

Table 2. List of the MMA and BA Polymerization Experiments and Their Conditions for Comparison of DLS and Mie Results[a]

	expt no.	C_M (M)	$C_M/C_{initiator}$ (M/M)	C_{SDS} (M)	D(v,0.5) (nm)	D_h (nm)
PMMA	1	0.458	290		173	208
	2	0.748	390		268	268
	3	0.458	292		133	196
	4	0.458	297	2.24×10^{-3}	111	80
	5	0.467	124		132	183
	6	0.467	126		135	180
PBA	1	0.273	92		141	218
	2	0.273	187		145	221
	3	0.268	46		246	259
	4	0.273	169		247	259
	5	0.273	165	2.24×10^{-3}	102	78

[a] D(v,0.5), mass median diameter (Mie scattering, Malvern MasterSizer) and z-averaged hydrodynamic diameter D_h (DLS, Brookhaven 90 Plus) for the end products of the reactions listed in Table 2. $K_2S_2O_8$ was used as initiator for all the reactions listed; $T = 70$ °C.

An important point in considering the SEC results here is that light scattering detection is used, rather than any column calibration using molecular weight standards. If the high mass molecules were eluting intact through the GCP columns, then they would be detected by the light scattering, which is not the case in this work. On the other hand, column calibration is unable to distinguish between high mass polymers eluting at low elution volumes and the lower standard masses expected to be eluting at these same elution volumes, from column calibration considerations. In fact, examination of the ln(M) vs elution profiles from the current data showed excellent linearity and do not display a positive upturn in mass at low elution volumes, as would be expected if very high mass polymers were eluting there.

The conclusion is that in emulsion systems where very high mass polymers are formed SEC may give an erroneous and underestimated molecular weight distribution when the large mass fraction does not elute, whether through chain shear degradation or trapping in the column. In contrast, the much lower shear ACOMP environment can keep even the larger polymers intact and give a more reliable value of M_w, $[\eta]_w$, and $\langle S^2\rangle_z$.

Comparison of Mie Scattering, DLS, and Cryo-TEM. Measurements of polymer latex particle size using both the Mie scattering (Malvern Master Sizer) and DLS (Brookhaven 90 Plus) are given in Table 2 for the end products of a series of reactions listed in the same table. There is fairly good agreement for the particle sizes for the two methods, although the average measured by each method are different types; DLS measures a z-averaged reciprocal hydrodynamic diameter, whereas the Mie value shown in Figure 8 is the mass median average of the population. The DLS "polydispersity index", defined as the ratio of the second moment to the first moment squared of the power series expansion of the electric field autocorrelation function, was very low, always less than 0.05, indicating a narrow size distribution. It was found in other experiments that as particle size drops below 100 nm, the Mastersizer was unable to report accurate sizes, whereas DLS continued to furnish reliable data (19 nm latex spheres could be accurately measured by DLS but not by the Mastersizer). On the other hand, DLS was unable to furnish reliable sizes above about 1 μm. Future work may involve use of both Mie scattering and DLS detectors in the ACOMP train.

Figure 10 shows a cryo-TEM image for pBA 3 (Table 2), a surfactant-free experiment. In agreement with the low DLS polydispersity index and narrow distribution from the Mie scattering, a fairly narrow range of particle diameters around 200 nm is seen. It was found that room temperature TEM led to fusing of the pBA latex particles, raising doubts about whether

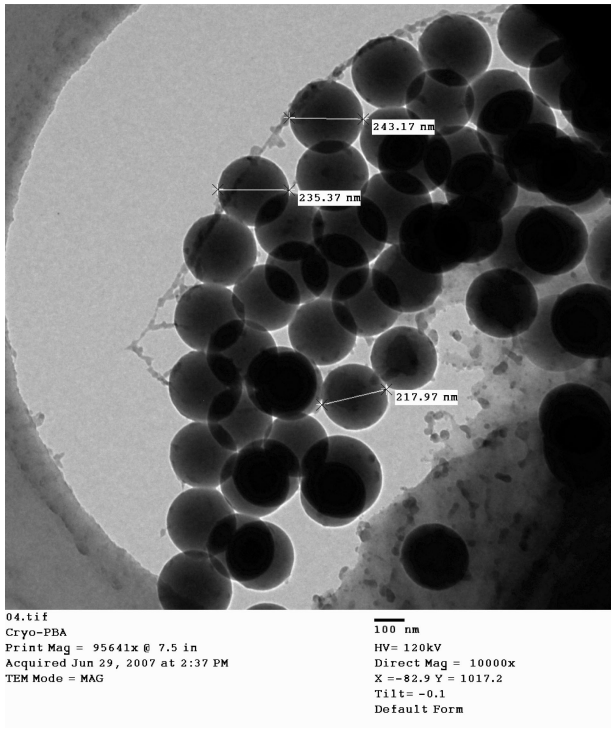

Figure 10. Cryo-TEM image for BA surfactant-free polymerization reaction ([BA] = 0.268M, pBA 3, Table 2).

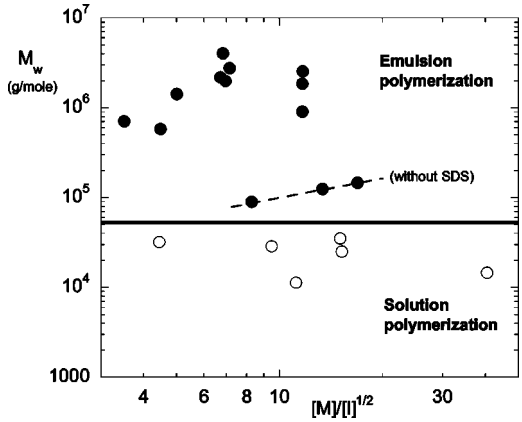

Figure 11. M_w vs $[M]/[I]^{1/2}$ (M is monomer and I is initiator) for the same types of MMA and BA homogeneous and emulsion polymerizations under different initiator conditions, showing the emulsion polymers are far larger than those produced in homogeneous phase.

there might be some interparticle latex aggregation in solution. The cryo-TEM shows that the latex particles are, in fact, distinct, and not fused in solution.

Comparison of Emulsion Polymerization with Homogeneous Phase Reactions. The current experiments confirm the well-known trend that emulsion polymerization is faster than under similar reagent concentrations in homogeneous phase and produces higher mass polymers. A comparison of polymerization rates (not shown) for BA and MMA in homogeneous phase shows the rates are typically several times lower than in emulsion, under similar reagent concentrations. Figure 11 shows M_w for MMA and BA end products from both emulsion and homogeneous phase polymerization where monomer/initiator ratios were similar, and different initiator concentrations were used. The M_w are seen to be dramatically higher for the emulsion polymerization reactions. The M_w for both MMA and BA in emulsion are lower when no SDS is present.

Summary

A new ACOMP platform has been developed that allows for simultaneous monitoring of the evolution of colloid phase (monomer droplets, polymer latex particles) and solution phase (polymer and monomer) characteristics during emulsion polymerization. The method has been applied here to MMA and BA homopolymerizations under a variety of concentration conditions, with and without surfactant. A number of features are captured by this process, such as multiphase conversion, the fast reaction time and large polymer masses produced, large changes in polymer average mass during synthesis, and a correlation between monomer droplet disappearance and monomer conversion. A comparison with homogeneous phase polymerization under similar conditions shows how greatly emulsion polymerization affects synthesis kinetics and polymer characteristics.

This is the first time particle sizing has been used in conjunction with ACOMP. Mie scattering results on average particle sizes were in good agreement with DLS and cryo-TEM measurements made on end products. Similarly, multidetector SEC measurements usually agreed with the results from the ACOMP "polymer side", where polymer and monomer characteristics were measured by homogenizing the emulsion via reactor content dilution with THF. The exception occurred when very large polymers are produced in the high concentration reactions. In this case ACOMP yields larger M_w and $\eta_{r,w}$ values than SEC, and it is suspected that this is due to shear degradation in the SEC columns. It is cautioned that in such cases traditional SEC approaches, especially those relying on column calibration, may give serious underestimates of polymer molar masses.

Integration of other particle sizing detectors into the ACOMP colloid detection train are planned, including flow equipped DLS (Brookhaven Instruments Corp.) and the use of heterogeneous time-dependent static light scattering (HTDSLS).[52] HTDSLS, through the counting of sharp scattering peaks from individual colloid particles passing through the scattering volume, should allow monitoring the number density and relative size of the monomer droplets as they are depleted and the nucleated polymer particles grow. This information will be a strong complement to the Mie scattering data.

The new instrumentation and methodology presented here have many potential uses. Plans are being made for extension to emulsion copolymerization, semibatch feed reactors, predictive control schemes, and the use of modern controlled radical polymerization reactions (ATRP, NMP, RAFT) to produce homopolymers and gradient and multiblock copolymers under "living-like" conditions.

Acknowledgment. This work was supported by Arkema Inc., Louisiana Board of Regents ITRS RD-B-05, NSF CBET 0623531, NASA NNC06AA18A, and the Tulane Center for Polymer Reaction Monitoring and Characterization (PolyRMC). Cryo-TEM images were produced by Alex Reed and Jibao He. We thank Dr. Chris Bertelo of Arkema Inc. for the suggestion of the redox couple initiation by *tert*-butyl hydroperoxide and sodium formaldehyde sulfoxylate used in experiment 2.

References and Notes

(1) Florenzano, F. H.; Strelitzki, R.; Reed, W. F. *Macromolecules* **1998**, *31*, 7226–7238.
(2) Giz, A.; Catalgil-Giz, H.; Alb, A. M.; Brousseau, J. L.; Reed, W. F. *Macromolecules* **2001**, *34*, 1180–1191.
(3) Alb, A. M.; Enohnyaket, P.; Shunmugam, R.; Tew, G. N.; Reed, W. F. *Macromolecules* **2006**, *39*, 8283–8292.
(4) Mignard, E.; Leblanc, T.; Bertin, D.; Guerret, O.; Reed, W. F. *Macromolecules* **2004**, *37*, 966–975.
(5) Alb, A. M.; Farinato, R.; Calbick, J.; Reed, W. F. *Langmuir* **2006**, *22*, 831–840.

(6) Harkins, W. D. *J. Chem. Phys.* **1945**, *13*, 381–387.
(7) Priest, W. J. *J. Phys. Chem.* **1952**, *56*, 1077–1082.
(8) Hansen, F. K.; Ugelstad, J. *J. Polym. Sci., Polym. Chem. Ed.* **1978**, *16*, 1953–1979.
(9) Reimers, J.; Schork, F. J. *J. Appl. Polym. Sci.* **1996**, *59*, 1833–1841.
(10) Feeney, P. J.; Napper, D. H.; Gilbert, G. G. *Macromolecules* **1984**, *17*, 2520–2529.
(11) Miller, C. M. S., E. D.; Silebi, C. A.; El-Aasser, M. S. *J. Polym. Sci., Part A: Polym. Chem.* **1995**, *33*, 1391–1408.
(12) Asua, J. M. *Prog. Polym. Sci.* **2002**, *27*, 1283–1346.
(13) El-Aaser, M. S.; Magawinita, T.; Misra, S.; Vanderhoff, J. W.; Pichot, C. *J. Polym. Sci., Polym. Chem. Ed.* **1983**, *21*, 2363–2382.
(14) Hamielec, A. E.; MacGregor, J. F.; Penlidis, A. *Makromol. Chem., Macromol Symp.* **1987**, *10/11*, 521–570.
(15) Arzamendi, G.; Leiza, J. R.; Asua, J. M. *J. Polym. Sci., Part A: Polym. Chem.* **1991**, *29*, 1549–1559.
(16) Canegallo, S.; Canu, P.; Morbidelli, M.; Storti, G. *J. Appl. Polym. Sci.* **1994**, *54*, 1919–1935.
(17) Canegallo, S.; Apostolo, M.; Storti, G.; Morbidelli, M. *J. Appl. Polym. Sci.* **1995**, *57*, 1333–1346.
(18) Santos, A. M.; Fevotte, G.; Othman, N.; Othman, S.; McKenna, T. F. *J. Appl. Polym. Sci.* **2000**, *75*, 1667–1683.
(19) Zeaiter, J.; Gomes, V. G.; Romagnoli, J. A.; Barton, G. W. *Chem. Eng. J.* **2002**, *89* (1–3), 37–45.
(20) Guyot, A.; Guillot, J.; Pichot, C.; Rios, L. In Emulsion Polymers and Emulsion Polymerization; Basset, D. R., Hamielec, A. E., Eds.; *ACS Symp. Ser.* **1981**, *165*, 415–436.
(21) Gossen, P. D.; MacGregor, J. F.; Pelton, R. H. *Appl. Spectrosc.* **1993**, *47*, 1852–1870.
(22) Reis, M. M.; Araujo, P. H. H.; Sayer, C.; Giudici, R. *Ind. Eng. Chem. Res.* **2004**, *43*, 7243–7250.
(23) Santos, A. F.; Silva, F. M.; Lenzi, M. K.; Pinto, J. C. *Pol.-Plast. Technol. Eng.* **2005**, *44*, 1–61.
(24) Chabot, P.; Hedhli, L.; Olmstead, C. *AT-PROCESS* **2000**, *5*, 1–6.
(25) Chatzi, E. G.; Kammona, O.; Kiparissides, C. *J. Appl. Polym. Sci.* **1997**, *63*, 799–809.
(26) Chai, X.-S.; Schork, F. J.; Oliver, E. M. *J. Appl. Polym. Sci.* **2006**, *99*, 1471–1475.
(27) Hua, H.; Dube, M. A. *J. Polym. Sci., Part A: Polym. Chem.* **2001**, *39*, 1860–1876.
(28) Elizalde, O.; Asua, J. M.; Leiza, J. R. *Appl. Spectrosc.* **2005**, *59*, 1280–1285.
(29) Henninger, B.; Pauer, W.; Moritz, H.-U. DECHEMA Monographien 2004, 138 (8th International Workshop on Polymer Reaction Engineering), **2004**, 329–333.
(30) Chien, D. C. H.; Penlidis, A. *J. Macromol. Sci., Rev. Macromol. Chem. Phys.* **1990**, *30*, 1–42.
(31) Hergeth, W. D. *Sens. Update* **1999**, *5*, 191–242.
(32) Asua, J. M. *J. Polym. Sci., Part A: Polym. Chem.* **2004**, *42*, 1025–1041.
(33) Urretabizkaia, A.; Sudol, E. D.; El-Aaser, M. S.; Asua, J. M. *J. Polym. Sci., Polym. Chem.* **1993**, *31*, 2907–2913.
(34) BenAmor, S.; Colombié, D.; McKenna, T. *Ind. Eng. Chem. Res.* **2002**, *41*, 4233–4241.
(35) Al-Khanbashi, A.; Dhamdere, M.; Hansen, M. *Appl. Spectrosc. Rev.* **1998**, *33*, 115–118.
(36) van den Brink, M.; Hansen, J. F.; De Peinder, P.; van Herk, A. M.; German, A. L. *J. Appl. Polym. Sci.* **2000**, *79*, 426–436.
(37) van den Brink, Pepers, M.; van Herk, A. M.; German, A. L. *Polym. React. Eng.* **2001**, *9*, 101–133.
(38) McCaffery, T. R.; Durant, Y. G. *Polym. React. Eng.* **2003**, *11*, 507–518.
(39) Jawhari, T.; Hendra, P. J.; Willis, H. A.; Judkins, M. *Spectrochim. Acta, Part A* **1990**, *46*, 161–170.
(40) Martens, H.; Naes, T. *Multivariate Calibration*; Wiley: New York, 1989.
(41) Vieira, R. A. M.; Sayer, C.; Lima, E. L.; Pinto, J. C. *Polymer* **2001**, *42*, 8901–8906.
(42) Reis, M. M.; Araujo, P. H. H.; Sayer, C.; Giudici, R. *Macromol. Rapid Commun.* **2003**, *24*, 620–624.
(43) Elizalde, O.; Leal, G. P.; Leiza, J. R. *Part. Part. Size Charact. J.* **2000**, *17*, 236–243.
(44) Edouard, D.; Sheibat-Othman, N.; Hammouri, H. *AIChE J.* **2005**, *5*, 3167–3185.
(45) McConville, J.; Tribe, K.; O'Donohue, S.; Saunders, G. Abstracts of Papers, 229th ACS National Meeting, San Diego, CA, March 13–17, 2005.
(46) Zimm, B. H. *J. Chem. Phys.* **1948**, *16*, 1093–1099.
(47) Kerker, M. *The Scattering of Light and Other Electromagnetic Radiation*; Academic Press: New York, 1969.
(48) Berne, B.; Pecora, R. *Dynamic Light Scattering*; John Wiley & Sons: New York, 1976.
(49) Koppel, D. E. *J. Chem. Phys.* **1972**, *11*, 4814–4823.
(50) Ahmad, N. M.; Heatley, F.; Lovell, P. A. *Macromolecules* **1998**, *31*, 2822–2827.
(51) Plessis, C.; Arzamendi, G.; Alberdi, J. M.; Van Herk, A. M.; Leiza, J. R.; Asua, J. M. *Macromol. Rapid Commun.* **2002**, *24*, 173–177.
(52) Schimanowski, R.; Strelitzki, R.; Reed, W. F. *Macromolecules* **1999**, *32*, 7055–7063.

MA7027825